# Signal Processing for Liquid Ionization Calorimeters*

W. E. Cleland and E. G. Stern

Department of Physics and Astronomy
University of Pittsburgh
Pittsburgh, PA 15260

FG02-91ER40646

ABSTRACT

We present the results of a study of the effects of thermal and pileup noise in liquid ionization calorimeters operating in a high luminosity environment. The method of optimal filtering of multiply-sampled signals which may be used to improve the timing and amplitude resolution of calorimeter signals is described, and its implications for signal shaping functions are examined. The dependence of the time and amplitude resolution on the relative strength of the pileup and thermal noise, which varies with such parameters as luminosity, rapidity and calorimeter cell size, is examined.

## 1. Introduction

Calorimeters operating at high luminosity colliders will very likely be read out by taking a number of samples of a shaped signal. A number of questions arise when considering the data acquisition and processing system for such a device, regarding the choice of shaping time, the number and position of the samples, and the required quantization accuracy. In this paper we show how the technique of optimal filtering can be used to evaluate the consequences of some of these design choices. A preliminary report of this study appeared in Ref. 1, and a more complete account is in preparation[2].

We begin by discussing the two noise sources, thermal and pileup, and define two quantities (thermal and pileup noise density) which are those factors in the expressions for noise which are independent of the signal processing. We then give a simple argument for finding the optimal shaping time in the presence of thermal and pileup noise. The expressions for optimal filtering are then developed, and analytical formulae for the variances for the amplitude and timing parameters in the limit of an infinite number of samples are given. The effects of quantization error are discussed, as well as some general remarks on the number and placement of the samples. Finally, we show the results of a Monte Carlo calculation in which the optimal filtering method is used to recover the parameters from simulated waveform data, including the effects of thermal and pileup noise.

In this paper we refer occasionally to our *standard case*, which is an $EM$ tower of area $\Delta\eta\Delta\phi = 0.04 \times 0.04$, located 75 cm from the interaction point. The value used for the thermal noise density $\rho_t$ (8 MeV$\sqrt{\text{ns}}$) is typical of a cell of a liquid argon calorimeter in the accordion geometry. We assume a drift time of 400 ns, and the shaping circuit with a measurement time $t_m$ of 50 ns. We assume the time constant associated with the preamplifier input stage of 2 ns. The assumed value of the pileup noise density $\rho_t$ is 3.75 MeV/$\sqrt{\text{ns}}$.

* Invited talk presented at III International Conference on Calorimetry, Corpus Christi, Sep 29-Oct 2, 1992

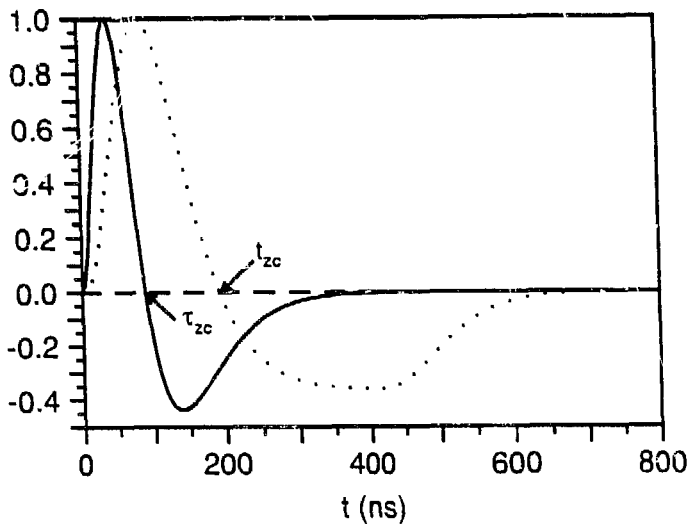


**Figure 2.1:** Shape of the impulse response $h(t)$ (solid curve) and the signal waveform $g(t)$ (dotted curve) for the standard case ($t_m$=50 ns, $t_d$=400 ns, $(RC)^2$-$(CR)^2$ shaping) used in this paper.

## 2. Sources of noise

The waveforms to be analyzed in this paper are those produced by the convolution of the current waveform from the liquid ionization chamber with the impulse response of the filter circuit in the electronics chain:

$$g(t) = \frac{1}{q_s} h(t) \star i(t) = \frac{1}{q_s} \int_{-\infty}^{\infty} i(t-u)\, h(u)\, du, \tag{2.1}$$

in which $h(t)$ is the impulse response, $i(t)$ the current waveform, and $q_s$ is the integrated signal charge, the constant required to make the first lobe of $g(t)$ equal to unity.

A useful quantity which characterizes the impulse response is the measurement time $t_m$, defined as[3]

$$t_m = \int_0^{\tau_{zc}} h(t)\, dt \tag{2.2}$$

and represents the effective integration time of the shaping circuit. In this expression $\tau_{zc}$ is the zero-crossing point of the first lobe of the impulse response (see Fig. 2.1). The electronic noise is expressed as the equivalent noise charge at the input of the preamplifier. For the case in which the capacitance of the preamplifier is not matched to the ionization chamber gap capacitance the relationship for the equivalent noise charge due to series noise is[4]

$$\overline{ENC^2} = \frac{1}{2} e_n^2 C_{tot}^2 I_1, \tag{2.3}$$

in which $e_n$ is the series noise voltage density for the amplifier, $C_{tot}$ is the sum of the detector capacitance and the channel capacitance of the transistor at the amplifier input, and $I_1$ is the series noise integral, which is related to the $\delta$-response of the circuit $h(t)$ as:

$$I_1 = \int_{-\infty}^{\infty} \left(\frac{dh}{dt}\right)^2 dt. \tag{2.4}$$

For a particle of energy $E_0$ incident on the front face of the calorimeter, the number of electrons generated in the gaps is

$$N_e = \frac{\eta_s E_0}{a_e W_{ion}},$$

in which $\eta_s$ is the sampling fraction, $a_e$ is the $\mu/e$ ratio, and $W_{ion}$ the ionization energy of the liquid. The ratio of $q_s$ to the total charge of the electrons generated in the gaps is related, to a good approximation, to $t_d$ and $t_m$ by[3]:

$$r_q = \frac{q_s}{q_e N_e} \approx \frac{t_m}{t_d} - \frac{1}{2}\left(\frac{t_m}{t_d}\right)^2 . \tag{2.5}$$

in which $q_e$ is the electronic charge.

Thus the thermal noise, expressed in energy units becomes

$$\sigma_t = \frac{E_0 \times ENC}{N_s} \tag{2.6a}$$

$$= \frac{1}{\sqrt{2}} \frac{e_n C_{tot} W_{ion} a_e}{\eta_s q_e} \frac{\sqrt{I_1}}{r_q}$$

$$= \rho_t \frac{\sqrt{I_1}}{r_q} . \tag{2.6b}$$

We have separated the above expression into two factors: $\rho_t$, the thermal noise density, which is independent of the signal processing parameters, and the other, $\sqrt{I_1}/r_q$, which is independent of all of the calorimeter constants except for $t_d$. The dimensions of $\rho_t$ are $E\sqrt{T}$.

The expression for the pileup variance is

$$\sigma_p^2 = \rho_p^2 T_c \sum_{i=-\infty}^{\infty} g^2(t_i) = \rho_p^2 \mathcal{S}_p \tag{2.7}$$

in which $\rho_p^2 = \mathrm{Var}(E)/T_c$ is the variance of the energy deposition in the calorimeter cell per crossing, $T_c$ is the time between crossings. The quantity $\rho_p$, called the pileup noise density, is that part of $\sigma_p$ which is independent of the signal processing parameters. The dimensions of $\rho_p$ are $\mathrm{E}/\sqrt{\mathrm{T}}$ while $\mathcal{S}_p$ has dimensions of T, reflecting the time interval over which pileup events contribute to the noise variance.

To estimate the effects of pileup, we use a Monte Carlo program to simulate the time structure of the machine by permitting collisions at points in time separated by the bunch crossing time and use Poisson statistics to determine the number of collisions of each type of events at each crossing. We consider only two jet (with transverse energy of the jet above 5 GeV) and minimum bias events, as generated in ISAJET version 6.21. The two types of events occur in approximately equal proportions.

Energy deposition in the calorimeter is simulated by the program[5] which employs the parameterization of Bock[6] for the electromagnetic and hadronic showers. We assume a spherical calorimeter of inner radius 75 cm with two depth segmentations: an electromagnetic section of thickness 25 radiation lengths and a hadronic section of 10 absorption lengths.

Once the transverse energy deposition for each calorimeter cell is determined, a sum for the cell $E_i$ over all events in a given crossing is made. We calculate $\rho_p$ by evaluating the quantity

$$\rho_p^2 = \frac{1}{T_c}\left[\frac{\sum_i E_i^2}{n} - \left(\frac{\sum_i E_i}{n}\right)^2\right] , \tag{2.8}$$

which is a characteristic of the sample of events contributing to the pileup. We have calculated $\rho_p$ for a range of values of the area of the calorimeter, from the size of individual cells ($\mathcal{A} = \Delta\eta \times \Delta\phi$=0.04 ×0.04 up to sizes comparable to or greater than that of jets. The results (see Fig. 2.2) leads one to the conclusion that $\rho_p \propto (\Delta\eta\Delta\phi)^{0.76}$ over a wide range of tower sizes. For uncorrelated noise, one would expect the variance to be linear in $\mathcal{A}$; this result indicates that the correlations in energy deposits due to the dominance of jet production significantly alters this naive expectation. We have also studied in the Bock parameterization the variation of pileup noise density with depth in the calorimeter, considering three segments of a hadron calorimeter, each 4$\lambda$ deep, located behind an EM section of depth 1$\lambda$. The values obtained, for a 0.04 ×

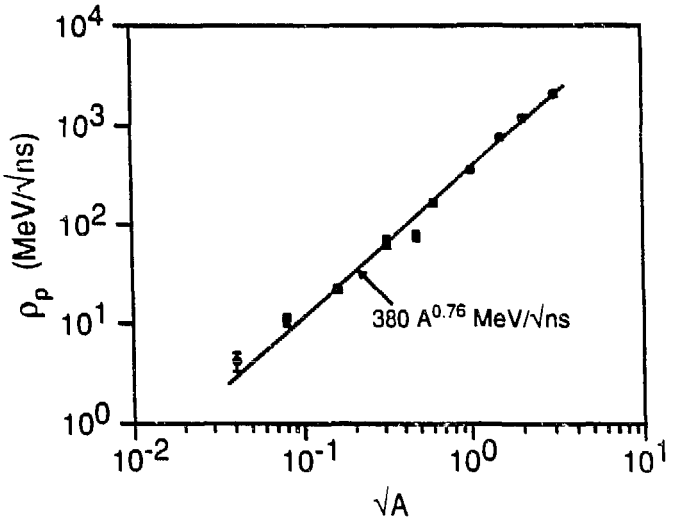


**Figure 2.2:** Monte Carlo-calculated pileup noise density (fluctuations in deposited transverse energy in a calorimeter cell) as a function of tower size $\sqrt{A} = (\Delta\eta\Delta\phi)^{1/2}$. The assumed luminosity is $L_0 = 10^{33}\text{cm}^{-2}\text{sec}^{-1}$.

0.04 tower, are 2.35, 0.43, and 0.033 MeV/$\sqrt{\text{ns}}$, respectively. These data may be roughly parameterized by $\rho_p \propto e^{\frac{-0.5\ell}{\lambda}}$, in which $\ell$ is the material between the interaction region and the face of the calorimeter section, and $\lambda$ is the interaction length of the material. We can combine these two scaling laws, along with the obvious linear dependence of the pileup variance with luminosity, and using the absolute value of the curve shown in Fig. 2.2, we arrive at an empirical formula for the pileup noise density:

$$\rho_p = 380\,(\Delta\eta\Delta\phi)^{0.76}\left(\frac{\mathcal{L}}{\mathcal{L}_0}\right)^{\frac{1}{2}} e^{\frac{-0.5\ell}{\lambda}}\,\text{MeV}/\sqrt{\text{ns}} \tag{2.9}$$

## 3. Optimal shaping time

Since the dependence of the noise on the measurement time is known, it is useful to consider whether one can achieve an optimum value for the shaping time by minimizing the noise. We consider the case for a calorimeter cell operating at a given luminosity, *i.e.* with $\rho_p$ and $\rho_t$ fixed. An intuitive choice for $t_m$ would be that value which minimizes $\sigma_s^2$, the variance of the signal including both pileup and thermal noise. This value can be easily found from the following argument. The expression for $\sigma_s^2$ is

$$\sigma_s^2 = \sigma_t^2 + \sigma_p^2 = \rho_p^2 S_p\,(t_m) + \rho_t^2 \frac{I_1\,(t_m)}{r_q^2\,(t_m)}, \tag{3.1}$$

in which $S_p$ is defined in Eq. (2.7), $I_1$ in Eq. (2.4), and $r_q$ in Eq. (2.5). To a good approximation, the functional dependencies of these quantities on $t_m$ is given by $I_1 = a_1/t_m$, $S_p = a_p t_m$, and $r_q = t_m/t_d$, in which $a_1$ and $a_p$ are dimensionless constants of order unity. This results in a simple expression for $\sigma_s$ as a function of $t_m$ which has a minimum at

$$t_m^0 = \left(\frac{3a_1}{a_p}\right)^{\frac{1}{4}} \sqrt{\frac{\rho_t t_d}{\rho_p}}. \tag{3.2}$$

and has for the value of the variance at the minimum

$$\sigma_{s0}^2 = 4\left(\frac{a_1 a_r^3}{27}\right)^{\frac{1}{4}}\sqrt{\rho_t t_d \rho_p^3}. \tag{3.3}$$

The numerical coefficient appearing in Eq. (3.2), $(3a_1/p_p)^{1/4}$, is very insensitive to the choice of $t_m$ or to $n$, the number of stages of integration in the filter. For the values of $t_m$ ranging from 20 ns to 200 ns and for n=2, 4, or 6, we find that this factor is within 5% of the value 1.5. Similarly, the numerical factor in Eq. (3.3) is within 10% of the value 3.7. Thus, to this level of accuracy, the two above equations become

$$t_m^0 \approx 1.5\sqrt{\frac{\rho_t t_d}{\rho_p}}, \tag{3.4}$$

$$\sigma_{s0} \approx \left(16\rho_t t_d \rho_n^3\right)^{\frac{1}{4}}. \tag{3.5}$$

## 4. Optimal filtering

We approach the problem of determining the amplitude and timing information from a set of measured samples by looking first at the traditional method for extracting information from an overdetermined data set: the $\chi^2$ method. We then turn to a solution from signal processing theory,[7] optimal filtering, and show that the two methods are equivalent to first order. This equivalence is particularly relevant for online data processing since optimal filtering calculations are ideally suited for implementation in hardware using digital signal processors.

We assume that the form of the signal at the output of the shaping amplifier is known, except for its amplitude $A$ and time origin $\tau$ (the deviation from the assumed crossing time). The expression for this signal is

$$S_i = Ag(t_i - \tau). \tag{4.1}$$

We also assume that the waveform will be sampled many times, giving a set of measurements $S_1, \ldots, S_n$. We wish to determine the parameters $A$ and $\tau$ from the data set $S_i$.

We define the $\chi^2$ function as follows :

$$\chi^2(A,\tau) = \sum_{ij}\left(S_i - Ag(t_i - \tau)\right)V_{ij}\left(S_j - Ag(t_j - \tau)\right) \tag{4.2}$$

in which $V_{ij}$ is the weight matrix for the measured points $S_i$. The dependence on $\tau$ is linearized by the use of a Taylor expansion:

$$g(t_i - \tau) = g(t_i) - \tau g'(t_i),$$

in which $g'(t) = dg/dt$. Defining the two parameters in the fit to be $\alpha_1 = A$ and $\alpha_2 = A\tau$, we have

$$\chi^2 = \sum_{ij}\left(S_i - \alpha_1 g_i + \alpha_2 g_i'\right)V_{ij}\left(S_j - \alpha_1 g_j + \alpha_2 g_j'\right)$$

where we have adopted the obvious notational convenience that $g(t_i) = g_i$ and similarly for $g'(t_i)$. We now form the following sums, expressed also in the equivalent matrix notation:

$$Q_1 = \sum_{ij} g_i V_{ij} g_j = \vec{g}^{+}\mathbf{V}\vec{g} \qquad Q_2 = \sum_{ij} g_i' V_{ij} g_j' = \vec{g}'^{+}\mathbf{V}\vec{g}'$$

$$Q_3 = \sum_{ij} g_i' V_{ij} g_j = \vec{g}'^{+}\mathbf{V}\vec{g} \qquad Q_4 = \sum_{ij} g_i V_{ij} S_j = \vec{g}^{+}\mathbf{V}\vec{S}$$

$$Q_5 = \sum_{ij} g_i' V_{ij} S_j = \vec{g}'^{+} \mathbf{V} \vec{S}.$$

In these equations $\vec{g}$ is the line vector of the unit-amplitude shaping function samples, $\vec{g}^{+}$ is its transpose, and $\vec{g}'$ is its time derivative. The line vector $\vec{S}$ is the set of measured data points. We set $\partial X^2/\partial \alpha_i = 0$, and solve the resulting linear equations for $\alpha_i$. The results are:

$$A \equiv \alpha_1 = \frac{1}{\Delta}\left[Q_2 Q_4 - Q_5 Q_3\right] \tag{4.3a}$$

$$A\tau \equiv \alpha_2 = \frac{-1}{\Delta}\left[Q_1 Q_5 - Q_3 Q_4\right], \tag{4.3b}$$

in which

$$\Delta = Q_1 Q_2 - Q_3^2.$$

### 4.1. Optimal filtering in the time domain

Optimal filtering refers to the formation of linear combinations of signal samples to recover the signal parameters, namely the amplitude $A$ and start time $\tau$, while maximizing the signal/noise ratio. We define coefficients $a$ and $b$ and form the linear sums $u$ and $v$ of signal samples $S$:

$$u = \sum_i a_i S_i, \qquad v = \sum_i b_i S_i. \tag{4.4}$$

We choose coefficients so that $u$ will be the amplitude $A$ of the signal, and $v$ will evaluate to $A\tau$. The shape of the signal is known, so that the samples $S_i$ will have values

$$S_i = A g\left(t_i - \tau\right) = A g_i - A\tau g_i' + n_i$$

where $n_i$ is a noise component and use has been made of the Taylor series expansion as before. We require the expectation value of $u$ to be $A$ and the expectation value of $v$ to be $A\tau$ so

$$A = \langle u \rangle = \sum_i \left(A a_i g_i - A\tau a_i g_i' + \langle n_i \rangle\right)$$

$$A\tau = \langle v \rangle = \sum_i \left(A b_i g_i - A\tau b_i g_i' + \langle n_i \rangle\right).$$

Since noise will average to 0, this leads to constraints on $a_i$ and $b_i$ that

$$\sum_i a_i g_i = 1 \qquad \sum_i a_i g_i' = 0 \qquad \sum_i b_i g_i = 0 \qquad \sum_i b_i g_i' = -1. \tag{4.5}$$

The variance of the parameters $u$ and $v$ is

$$\begin{aligned} Var\left(u\right) &= \sum_{ij} a_i a_j \langle n_i n_j \rangle = \sum_{ij} a_i a_j R_{ij} \\ Var\left(v\right) &= \sum_{ij} b_i b_j \langle n_i n_j \rangle = \sum_{ij} b_i b_j R_{ij} \end{aligned} \tag{4.6}$$

after performing the subtraction and setting $\langle n_i \rangle = 0$. The expectation value $\langle n_i n_j \rangle = R_{ij}$ is the noise autocorrelation function evaluated at time $t_i - t_j$.

We minimize the variances of u and $v$ while satisfying the constraints of Eq. (4.5) using Lagrange multipliers. The functions to be minimized are:

$$I_u = \sum_{ij} R_{ij} a_i a_j - \lambda \left( \sum_i a_i g_i - 1 \right) - \kappa \sum_i a_i g_i' \tag{4.7a}$$

$$I_v = \sum_{ij} R_{ij} b_i b_j - \mu \sum_i b_i g_i - \rho \left( \sum_i b_i g_i' + 1 \right) \tag{4.7b}$$

and $\lambda$, $\kappa$, $\mu$ and $\rho$ are the Lagrange multipliers. Proceeding in the usual fashion and setting the partial derivatives with respect to $a_i$ and $b_i$ to 0 gives a set of linear equations which can be expressed in matrix form. In this form, the solution for $\vec{a} \equiv a_i$ and $\vec{b} \equiv b_i$ is:

$$\vec{a} = \lambda \mathbf{V} \vec{g} + \kappa \mathbf{V} \vec{g}' \qquad \vec{b} = \mu \mathbf{V} \vec{g} + \rho \mathbf{V} \vec{g}'. \tag{4.8}$$

The matrix $\mathbf{V}$ is the inverse of the autocorrelation matrix $\mathbf{R} \equiv R_{ij}$ and is the same matrix that appears in Eq. (4.2) as the weight matrix of the signal samples. The Lagrange multipliers can be determined from the constraint equations. The solution, in the notation introduced above, is

$$\lambda = \frac{Q_2}{\Delta} \qquad \kappa = \frac{-Q_3}{\Delta} \qquad \mu = \frac{Q_3}{\Delta} \qquad \rho = \frac{-Q_1}{\Delta} \tag{4.9}$$

where $\Delta = Q_1 Q_2 - Q_3^2$. Substitution of Eqs. (4.9) into equations (4.8) and (4.4) yields the same results as were given previously in Eqs. (4.3) for the general first order $\chi^2$ method. Thus we see that the requirement of minimizing the variances of the parameters $A$ and $A\tau$ and minimizing the $\chi^2$ function to first order lead to the same results.

An important property of the optimal filter technique is that the variance of either the amplitude or timing parameter becomes much less sensitive to the shaping time than $\sigma_s$. To illustrate this point, we show in Fig. 4.1 the comparison between $\sigma_s$ and $\sigma_A$ as a function of $t_m$ for the case where the samples are taken each 16 ns over the entire waveform. As the number of samples is reduced to a practical value, the sensitivity to $t_m$ increases, and the curves lie in between the two curves shown in Fig. 4.1. This independence on $t_m$ can be easily understood by considering the filtering process in the frequency domain.

Since we are dealing with a system which is bandwidth limited by the shaping amplifier, data samples taken in a time which is short compared to the dwell time of the shaped signal are correlated. It is necessary, when considering the treatment of highly correlated data, to understand the autocorrelation function for the system[8], from which we can obtain the covariance matrix matrix for the data samples, which is a Toeplitz matrix constructed from the autocorrelation function. We see above that the autocorrelation function enters naturally into the optimal filter formalism, and, as we mention above, this matrix is also employed in the $\chi^2$ method, since the weight matrix is the simply the inverse of the covariance matrix. In our case, we have two sources of noise; thermal noise contributes a series noise and gives an autocorrelation function $R_t$, while pileup noise gives a parallel noise with an autocorrelation function $R_p$. These two autocorrelations are summed to give a total autocorrelation function $\langle n_i n_j \rangle = R(t_i - t_j) = R_t(t_i - t_j) + R_p(t_i - t_j)$. The function $R_t$ is the series (thermal noise) autocorrelation function, given by

$$R_t(t) = \frac{\rho_t^2}{r_q^2} \int_{-\infty}^{\infty} h'(t+u)\, h'(u)\, du, \tag{4.10}$$

in which $h' = dh/dt$. The function $R_p$ is the autocorrelation function for pileup noise:

$$R_p(t) = \rho_p^2 \int g(t+u)\, g(u)\, du. \tag{4.11}$$

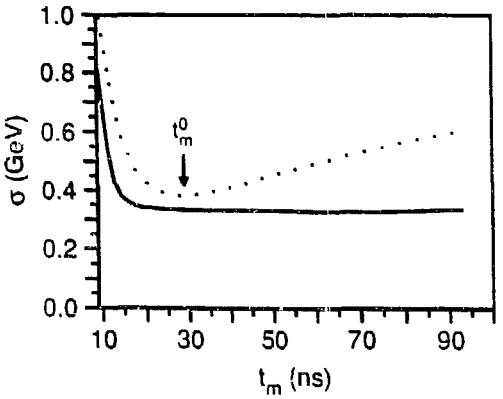


**Figure 4.1:** Noise value $\sigma_s$ (dotted curve) for a 5×5 sum of 0.04 ×0.04 EM cells operating at standard conditions, compared with the values of $\sigma_A$ (solid curve) obtained from optimal filtering for sampling of the full waveform each 16 ns. Use of a smaller number of samples produces a curve intermediate between these two.

## 4.2. Weighting function

In order to understand the implications of the solutions found above, we describe here the weighting function appropriate to the problem. Recall that in Eqs. (4.8) and (4.9), we have found expressions for the coefficients $a_i$ and $b_i$ such that:

$$A = \sum_i a_i S_i \qquad \tau = \frac{1}{A} \sum_i b_i S_i . \tag{4.12}$$

Because these equations are simply a direct function of the measured signal ( i.e. no convergence criterion is needed for their solution, as is the case for an iterative $\chi^2$ solution), it is possible to define a response function for the system as a function of its time origin. The weighting function is defined as the value of $A$ or $A\tau$ for unit energy deposited at time $t$ in the calorimeter cell. To find and expression for this function, we replace $S_i$ by the unit amplitude response, shifted in time by an amount $t$:

$$y_A(t) = \sum_i a_i g(t_i - t) . \tag{4.13}$$

We can view the weighting function as a measure of the response of the system to out-of-time signals. The effective width of the weighting function is defined as the width of a rectangle of unit height whose area is the integral of the square of the function. By definition $y_A(0)$ is unity. The effective width of the weighting function, for our case is given by

$$\begin{aligned} W &= \int_{-\infty}^{\infty} y_A^2(t)\, dt = \int_{-\infty}^{\infty} \left[ \sum_i a_i\, g(t_i - t) \right]^2 dt \\ &= \sum_{ij} a_i a_j \int_{-\infty}^{\infty} g(u)\, g(t_j - t_i + u)\, du \\ &= \frac{1}{\rho_p^2} \sum_{ij} a_i a_j R_p(t_i - t_j) , \end{aligned} \tag{4.14}$$

where the latter substitution comes from Eq. (4.11). From Equation (4.6) we see that

$$\sigma_A^2 = Var(A) = \sum_{ij} a_i a_j R_t(t_i - t_j) + \sum_{ij} a_i a_j R_p(t_i - t_j) \tag{4.15a}$$

$$= \xi_t + \xi_p = \xi_t + \rho_p^2 W, \tag{4.15b}$$

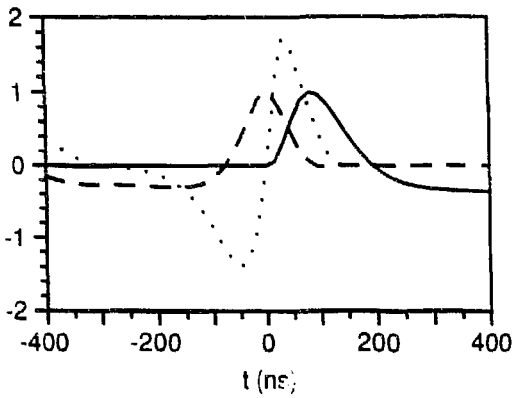


**Figure 4.2:** Weighting functions for the amplitude (dashed curve) and timing (dotted curve) parameters for our standard case. This signal waveform (solid curve) is shown for comparison.

in which $\xi_t$ and $\xi_p$ are the components of the variance of $A$ due to thermal and pileup noise, respectively. By comparison with Eq. (2.7), we see that the effective width of the weighting function $W$ plays the same role as the pileup sum $S_p$ plays for the variance of a single data point. It is this property of the weighting function which makes it useful in the discussion of pileup noise.

We see, therefore that the shape of the weighting function for a solution for the $a_i$ and $b_i$ gives an indication of the relative importance of thermal and pileup noise. The weighting function for a solution in which pileup is the dominant component of the noise will be narrower than one in which thermal noise dominates.

The weighting function for the time offset parameter $\tau$ is found by an analogous argument:

$$y_\tau(t) = \sum_i b_i g(t_i - t). \tag{4.16}$$

This function has two properties which can be verified by inspection of the constraint equations Eq. (4.5). One is that $y_\tau(0)=0$, and the other is that $y'_\tau(0)=1$, so that the magnitude of the weighting function for a signal displaced by an amount $\tau$ is simply equal to $\tau$. The curve of $y_\tau(t)$ *vs.* $t$ shows the region over which the optimal filtering method is able to determine the time offset. As is shown in Section 4.3, $y_\tau(t)$ is proportional to $y'_A(t)$, which is an important property when considering possible online applications of optimal filtering.

In summary, we see that the weighting function characterizes the signal processing operations of the system, and that its width, defined in Eq. (4.14) is a convenient parameter for describing the effects of signal processing on the contribution of pileup noise. The weighting functions for both the amplitude and timing parameters for our standard case are shown in Fig. 4.2.

### 4.3. Optimal filtering in the frequency domain

The optimal filtering problem can equivalently be considered in the frequency domain and offers a simple explanation for the behavior illustrated in Fig. 4.1. The formalism for frequency domain filters is developed by Papoulis [7], where it is shown that for a signal with (complex) frequency spectrum $G(\omega)$, the Fourier transform of $g(t)$, and a noise power spectrum $S(\omega)$, the filter $\mathcal{H}(\omega)$ that maximizes signal/noise at $t = 0$ has a frequency response

$$\mathcal{H}_A(\omega) = \frac{K_A G^*(\omega)}{S(\omega)} \tag{4.17}$$

where $G^*$ is the complex conjugate of $G$ and $K_A$ is a multiplicative constant to normalize the filtered signal, which, for an unknown signal $U(\omega)$ is given by the inverse Fourier transform evaluated at t=0:

$$A = \frac{1}{2\pi}\int_{-\infty}^{\infty} U(\omega)\,\mathcal{H}_A(\omega)\,d\omega. \tag{4.18}$$

We wish to normalize the filter so that it gives it gives unit amplitude for the peak when operating on the unit waveform $g(t)$ with spectrum $G(\omega)$. This gives the condition that

$$\frac{1}{K_A} = \frac{1}{2\pi}\int_{-\infty}^{\infty} \frac{|G(\omega)|^2}{S(\omega)}\, d\omega. \tag{4.19}$$

The weighting function for the filter is the response of the filter to a signal of unit amplitude as a function of time. In the frequency domain, shifting a function by amount $t$ corresponds to multiplying its spectrum by the factor $e^{j\omega t}$. Thus the weighting function is obtained by inserting this factor into Eq. (4.18):

$$y_A(t) = \frac{K_A}{2\pi}\int_{-\infty}^{\infty} \frac{|G(\omega)|^2}{S(\omega)} e^{j\omega t}\, d\omega. \tag{4.20}$$

We note that our normalization procedure gives the weighting function unit amplitude at $t = 0$.

Since $|\mathcal{H}_A|^2 S$ is the spectral density of the filtered noise, the variance of the filtered signal is

$$\sigma_A^2 = \frac{1}{2\pi}\int_{-\infty}^{\infty} |\mathcal{H}_A(\omega)|^2 S(\omega)\, d\omega = \frac{1}{2\pi} K_A^2 \int_{-\infty}^{\infty} \frac{|G(\omega)|^2}{S^2(\omega)} S(\omega)\, d\omega = K_A. \tag{4.21}$$

Similar considerations can be used to find the optimal filter for the time offset parameter $\tau$, and there one finds for the weighting function

$$y_\tau(t) = \frac{K_\tau}{2\pi}\int_{-\infty}^{\infty} \frac{j\omega |G(\omega)|^2}{S(\omega)} e^{-j\omega t}\, d\omega \tag{4.22}$$

Following the same reasoning used in Eq. (4.21), we find for the variance

$$\frac{1}{A^2\sigma_\tau^2} = \frac{1}{2\pi}\int_{-\infty}^{\infty} \frac{\omega^2 |G(\omega)|^2}{S(\omega)}\, d\omega = \frac{1}{K_\tau}. \tag{4.23}$$

From Eq. (4.20) and Eq. (4.22) one sees that $y_A$ and $y_\tau$ are related by

$$y_\tau(t) = -\frac{K_\tau}{K_A} y_A'(t) = -\left(\frac{A\sigma_\tau}{\sigma_A}\right)^2 y_A'(t). \tag{4.24}$$

It can also be easily verified from Eq. 4.22 and 4.20 that at $t = 0$, $y_\tau' = 1$, as required from its definition.

Besides providing an intuitive understanding of optimal filters, the frequency domain formalism permits us to derive general properties of optimal filters that are not evident in the time domain formulation. As we have developed optimal filtering in the frequency domain, we have required integration over all frequencies. In the time domain, this corresponds to integration over all times and sampling the signal at infinitely small time intervals. We refer to this unphysical situation as the "infinite sampling limit" (ISL). Values of $\sigma_A$ and $A\sigma_\tau$ calculated in this limit represent *lower limits* to values obtainable in reality. A situation somewhat closer to reality is found by integrating the function between fixed limits. This represents the situation in which the signal is sampled periodically and all of the samples are analyzed, and is called the "full sampling limit" (FSL). Although space does not permit a discussion of this point, we illustrate in Fig. 4.3 the curves that are obtained in this limit as well as the curves found for two realistic sampling patterns.

We now derive analytical expressions for the variances of the parameters $A$ and $A\tau$ in the infinite sampling limit. By using Parseval's theorem, it is straightforward to write the spectral density $S(\omega) = S_i(\omega) + S_p(\omega)$ in terms of the constants we have already introduced:

$$S_p(\omega) = \rho_p^2 |G(\omega)|^2 = \frac{\rho_p^2}{q_s^2} |I(\omega)|^2 |H(\omega)|^2 \tag{4.25}$$

and

$$S_t(\omega) = \frac{\rho_t^2 \omega^2}{r_q^2} |H(\omega)|^2, \tag{4.26}$$

in which $H(\omega)$ is the Fourier transform of $h(t)$ and $I(\omega)$ is the Fourier transform of the current waveform $i(t)$. From Eq. (4.21), and recalling that $r_q = q_s/q_e N_e$, we find:

$$\begin{aligned}
\frac{1}{\sigma_A^2} &= \frac{1}{2\pi} \int_{-\infty}^{\infty} \frac{|G(\omega)|^2}{S_p(\omega) + S_t(\omega)} d\omega \\
&= \frac{1}{2\pi} \int \frac{\frac{1}{q_e^2} |I(\omega)|^2 |H(\omega)|^2}{\frac{\rho_p^2}{q_e^2} |I(\omega)|^2 |H(\omega)|^2 + \frac{\rho_t^2}{r_q^2} \omega^2 |H(\omega)|^2} d\omega \\
&= \frac{1}{2\pi} \int_{-\infty}^{\infty} \frac{\left(\frac{1}{q_e N_e}\right)^2 |I(\omega)|^2}{\left(\frac{\rho_p^2}{q_e N_e}\right)^2 |I(\omega)|^2 + \rho_t^2 \omega^2} d\omega
\end{aligned} \tag{4.27}$$

It is the cancellation of $|H(\omega)|^2$ in this equation that explains why the optimal filtering method is insensitive to the value of $t_m$.

In carrying out the solution, we find that it is useful and reasonably accurate to approximate the quantity $|I(\omega)|^2/q_e^2 N_e^2$ by its first term $1/\omega^2 t_d^2$. The solution becomes an integral of the form

$$\begin{aligned}
\frac{1}{\tilde{\sigma}_A^2} &= \frac{1}{2\pi} \int_{-\infty}^{\infty} \frac{\frac{1}{\omega^2 t_d^2}}{\frac{\rho_p^2}{\omega^2 t_d^2} + \rho_t^2 \omega^2} d\omega \\
&= \frac{1}{2\pi} \int_{-\infty}^{\infty} \frac{1}{\rho_p^2 + \rho_t^2 t_d^2 \omega^4} d\omega \qquad (4.28a) \\
&= \frac{1}{2\pi \sqrt{t_d \rho_t \rho_p^3}} \int_{-\infty}^{\infty} \frac{du}{1 + u^4} \qquad (4.28b)
\end{aligned}$$

where we have made the substitution $u = \omega \sqrt{t_d \rho_t / \rho_p}$. The integral has the value of $\pi/\sqrt{2}$, so

$$\tilde{\sigma}_A^2 = \sqrt{8\, t_d\, \rho_t\, \rho_p^3}. \tag{4.29}$$

All quantities calculated in the ISL are designated with a tilde ($\sim$). By comparing this result with Eq. (3.5) we see that the maximum factor by which optimal filtering will improve the value of $\sigma_A$ over $\sigma_0$ is $2^{1/4}$=1.19 if the hardware shaping time is equal to the optimum value $t_m^0$.

The noise for the timing parameter can also be calculated the same way starting from Eq. (4.23) and proceeding in a similar way. We find

$$A^2 \tilde{\sigma}_\tau^2 = \sqrt{8 t_d^3\, \rho_t^3\, \rho_p}. \tag{4.30}$$

Note that these results are independent of the shaping time of the impulse response function and are valid only for situations where both thermal and pileup noise are present. By evaluating the portion of the variance $\sigma_A^2$ which comes from the pileup noise and comparing with Eq. (4.15), we can obtain a value for the effective width of the weighting function in the ISL:

$$\tilde{W} = 3 \sqrt{\frac{t_d \rho_t}{2 \rho_p}}. \tag{4.31}$$

The region of validity of the ISL formulae can be expressed in terms $\tilde{W}$: the ISL formulae are a poor approximation to the values of $\sigma_A$ and $A\sigma_\tau$ if $\tilde{W} < T_c$, where pileup noise dominates, or $\tilde{W} > t_{zc}$ (see Fig. 2.1), where thermal noise dominates.

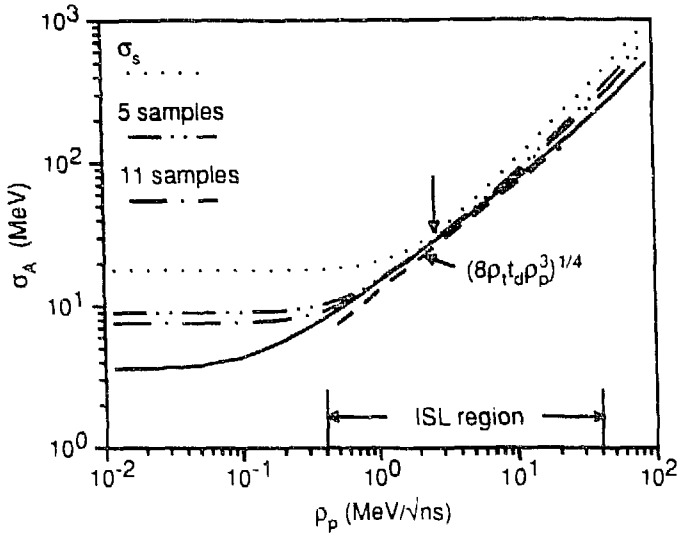


**Figure 4.3:** Amplitude resolution *versus* the pileup noise density. The vertical arrow indicates that point where $t_m = t_m^0$. The dotted curve is the total noise $\sigma_s$. The FSL solution (solid curve), sets a lower limit to the value of $\sigma_A$ which can be achieved with sampling the entire waveform. The two sampling patterns used are described in Section 5.

The way in which the ISL expression for $\sigma_A$ approximates the FSL integral and the values of $\sigma_A$ obtained for a small number of samples is illustrated in Fig. 4.3 . In this figure, we show $\sigma_A$ at a fixed value of $\rho_t$ and $t_d$, varying the value of $\rho_p$ over a wide range. In a more general sense, the plot shows the behavior of the system as a function of (1) luminosity ($\rho_p \propto \mathcal{L}^{\frac{1}{2}}$), with luminosity increasing to the right, (2) depth in the calorimeter, increasing to the left, and (3) area of the tower size, increasing to the right ($\rho_p \propto \mathcal{A}^{0.76}$, while $\rho_t \propto \mathcal{A}^{0.5}$).

## 5. Data acquisition considerations

The design of the data acquisition electronics for a large calorimeter system requires a number of interrelated design choices, and optimal filtering formalism may helpful in evaluating them. For example, it is shown in Section 4.3 that the degree to which one wishes to depart from the optimum shaping time impacts the question of the number of samples needed.

How many samples are needed and how to place them requires a detailed investigation of the particular situation of interest. In this brief report, we will confine our remarks to a few general statements. In Fig. 4.3 we compare the results of two sampling patterns for our standard case, one with 11 samples and the other with 5 samples. For the former, the samples are made each 16 ns over the entire first lobe of the waveform. The latter is the same sampling pattern, with every other sample missing.

A single sample with $t_m = t_m^0$ yields a value of $\sigma_A$ which is within 20% of that achieved by full sampling, and therefore the benefits of multiple sample are minimal. Multiple sampling is more useful in cases where: (a) shaping times are nonuniform due to variation of parameters in the manufacture of integrated circuits; (b) it is required to operate the calorimeter of a wide range of machine luminosity; (c) non-optimal shaping is used for reasons of convenience, *i.e.* by installing circuits of similar shaping times in regions of the calorimeter with significantly different values of $t_m^0$; and (d) timing information of individual calorimeter cells is important for offline background rejection. Depending on which of these criteria dominate the design, different choices for the number and position of the samples may be made. When $t_m$ is not close to $t_m^0$, it is possible to obtain values of $A$ and $\tau$ from optimal filtering with an uncertainty significantly lower than that of a single sample.

We now turn to the question of how the quantization accuracy of the digitization of the samples $S_i$ affects the variance of the parameters. Intuitively one suspects that if there are large negative values of the filter coefficients, indicating that the final value of the parameter is the result of the subtraction of two large numbers, there may be increased sensitivity to the quantization error. It is easy to show that this is in fact the case. We first consider the value of the quantization error in the digitization of the $S_i$. If we assume that a linear scale is used, with a maximum value of $E_{\max}$, then for a precision of $N$ bits, the quantization error in $S_i$ is $\sigma_q = E_{\max}/\sqrt{12}(2^N - 1)$. The result from Section 4.2 show that the amplitude $A$ and the time shift $\tau$ are related to the samples $S_i$ by linear expressions (see Eq. (4.12)). The propagation of the quantization error to the fitted parameters is straightforward:

$$q_A = \sigma_q \sqrt{\sum a_i^2} = \sigma_q R_A \qquad A q_\tau = \sigma_q \sqrt{\sum b_i^2} = \sigma_q R_\tau, \tag{5.1}$$

in which $q_\alpha^2$ is the contribution of the quantization error to the variance of parameter $\alpha$.

We have found that for a certain patterns, values of $R_A$ can be as low as 0.5, indicating that effectively 1 bit of precision can be gained through a judicious choice of the sample positions. However, the precision can be also be seriously compromised for pathological sample patterns. A useful parameter to examine for this purpose is the effective width of the weighting function. Following the argument given above, we expect that when the coefficients results in large difference terms, the value of $R_A$ will be large. This type of subtraction occurs if the filter reduces the width of the weighting function significantly below the hardware shaping time. Thus one expects a dependence of $R_A$ and $R_\tau$ on $\tilde{W}$. It is found that for the case of a small number of samples, when the effective width becomes less than $\tilde{W}$, both $R_A$ and $R_\tau$ become very large, as intuitively expected. Thus although the effective width of the weighting function can become quite small, this is not a practical way to reduce the pileup contribution, because of the increased contribution of the quantization error to the variance. This effect is more severe, the smaller the number of samples.

To give an indication of the size of the quantization errors, we calculate $\sigma_q$ for a typical case for operation at the SSC. There one needs in the EM cells a value of $E_{max}$ of approximately 2.5 TeV, so if one digitizes with a precision of 16 bits, $\sigma_q$= 11 MeV. For the standard case we have been considering, the sampling pattern with 5 samples yields values of $R_A$=0.94 and $R_\tau$= 57 ns, so the quantization errors in the parameters become $q_A$= 10 MeV and $Aq_\tau$=0.62 GeV-ns, small compared to the "noise" errors on the parameters $\sigma_A$=38 MeV and $A\sigma_\tau$=1.4 GeV-ns but not totally negligible. Clearly the quantization errors could become dominant if one uses solutions with values of $R_A$ or $R_\tau$ significantly larger than these or if lower precision is chosen for the ADC.

## 6. Monte Carlo Tests

In order to verify some of the results obtained in this paper, we have written a Monte Carlo program to simulate the addition of the thermal and pileup noise to a shaped signal of known amplitude, and then to reconstruct the amplitude using the optimal filtering method. The model for thermal noise approximates the actual noise generation process by an amplitude distribution of a Gaussian shape with a width $\rho_t$ and multiplying this amplitude by $h'(t)$. The interval chosen for the origination of the waveforms is the period of the machine clock (16 ns), but it is necessary to integrate the Poisson distribution between crossings to obtain the fluctuations for a noise source continuously distributed in time. For the pileup noise, the procedure for calculating the distribution of energy deposition in a calorimeter cell is discussed in Section 2, and the resulting histogram for one cell is shown in Fig. 6.1a. The large spike at zero is a consequence of the low occupancy for a small cell. As is discussed in Section 2 we characterize this distribution with its variance and, after combining it in quadrature with $\sigma_t$, proceed to treat the quantity $\sigma_s$ as if it were a Gaussian-distributed quantity (*e.g.* for the $X^2$ analysis). We wish to test the degree to which we can rely upon the central limit theorem for this procedure.

We work with two distributions for the pileup noise: $f_{NG}(E)$, which is the non-Gaussian histogram of Fig. 6.1a, and a Gaussian distribution $f_G(E)$ with the same mean and variance as $f_{NG}$. In either case $E$ represents the pileup energy seen in a calorimeter cell for one machine crossing, where the number of interactions is assumed to be Poisson distributed with a mean of 1.6 events. The random variable $E$ is then

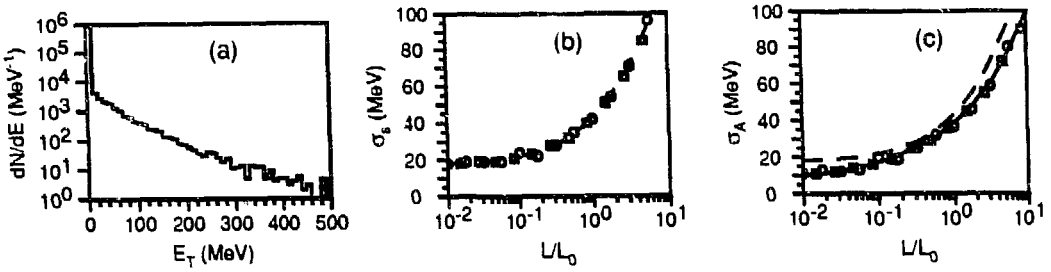


**Figure 6.1:** (a)Distribution of transverse energy seen in one EM cell of size 0.04 × 0.04 per crossing. (b)Monte Carlo data for the value of $\sigma_s^{mc}$ as a function of luminosity. The squares are data taken from the data of (a), and the circles are for data taken from a Gaussian distribution with the same mean and variance. The dashed curve is calculated from the formula $\sigma_s^2 = \sigma_t^2 + \sigma_p^2$. (c)Monte Carlo data for $\sigma_A^{mc}$, with the meaning for the symbols described for (b). The dashed curve is the calculated value for $\sigma_s$ shown in (b) and the solid curve is the value for $\sigma_A$ expected from the optimal filter method using 5 samples.

multiplied by the signal waveform $g(t)$, and we proceed to the next crossing. At any crossing the total noise signal $n(t)$ is found by adding together the thermal and pileup signals from all previous crossings occurring within the deviation of the signal waveform $g(t)$. We calculate $\sigma_s^{mc} = \sqrt{\mathrm{Var}(n)}$ for comparison with the expected value $\sigma_s^2$ from Eq. (3.1).

At a specific crossing, after the stationary value of $n(t)$ is reached (*i.e.* after the duration of the signal $g(t)$), a signal waveform of a given energy $E_0$ is simulated by generating a waveform $U(t) = E_0 g(t)$. To this signal is added the noise signal $n(t)$ at each crossing. For the reconstruction phase, a mask is used to pick those crossings that are to be sampled. We give results of a pattern with 5 samples, similar to what would be used in an offline analysis. The optimal filter coefficients, are then used to find the noise-distorted values of the amplitude and timing parameters for each event. After processing a sample of events the variances $\mathrm{Var}(A)$ and $\mathrm{Var}(A\tau)$ are calculated. The identical procedure is carried out for both pileup distributions $f_{NG}(E)$ and $f_G(E)$.

We test our procedure of the pileup noise generation by sampling the baseline for the case where there is no thermal noise and no signal present. In this case we expect the variance of the baseline to be given by Eq. (2.7). The value of the pileup noise density from the histogram of Fig. 6.1a is $\rho_p$=3.7 MeV/$\sqrt{\mathrm{ns}}$, and the value of $S_p$ is found to be 104 ns. This yields $\sigma_p = \rho_p\sqrt{S_p T_c} = 37.3$MeV, at $\mathcal{L} = \mathcal{L}_0$. From our Monte Carlo procedure, we find the value 37.7 ± 2.6 MeV, in good agreement with the expected value.

The remainder of the study is to carry out the procedure outlined above, finding Monte Carlo values for $\sigma_s^{mc} = \sqrt{\mathrm{Var}(n)}$, and $\sigma_A^{mc} = \sqrt{\mathrm{Var}(A)}$, which are shown in Fig. 6.1. We choose to display these quantities as a function of luminosity, passing from the region where $\sigma_t \gg \sigma_p$ to the region where $\sigma_t \ll \sigma_p$. If there were an important effect due to the non-Gaussian nature of the pileup noise, one would expect to see a difference between the two data sets at high luminosity. No such effect is seen at the level of statistical accuracy of these simulations, which is a few percent.

## 7. Summary and Conclusions

The main point of this work has been to show the utility of measuring multiple samples on a shaped waveform and combining them to find values of the unknown parameters $A$ and $A\tau$. The principal conclusion is that when the value of the shaping time is chosen to give the minimum value for a particular level of pileup and thermal noise, the error in $A$ found from measuring one sample at the peak is very close (typically within 20 %) of that which can be achieved by measuring any number of samples on the waveform. The main advantage in multiple sampling comes in cases where the shaping time is not the optimal one. The optimum filter method, in effect, redefines the shaping time numerically and therefore permits one to come close to optimal value for the error even though one may be rather far from the optimal hardware shaping time.

There are limits to how well the method can work, which become more restrictive as the number of samples is decreased. The precision of the measurement can be seriously compromised if the hardware shaping time $t_m$ is significantly longer than the optimal value, as the quantization error may become quite significant. This occurs since the digital filtering method effectively creates the difference between two large numbers in coming to its solution, as is discussed in Section 5.

We have introduced expressions for the variances of the parameters $A$ and $A\tau$ found by optimal filtering in the infinite sampling limit (ISL). These are analytic expressions found using the frequency domain formalism, and they can be visualized as the values which would be obtained if one could take infinitely many samples over the entire waveform. These expressions are useful both because they represent limits which can be approached in any practical situation and also because in many cases of practical interest, where both pileup and thermal noise are present, they approximate the practical solution to within about 20 percent. Quantities calculated in this limit are designated by a tilde($\sim$).

The use of optimal filtering permits a rapid calculation of the parameters with coefficients that can be determined from a knowledge of the thermal and pileup noise in the calorimeter. For this reason it is an algorithm well suited to online applications, as for example in a calorimeter trigger system. The properties of the weighting functions $y_A(t)$ and $y_\tau(t)$, which can be generated in real time in a digital processor, can be used to establish both the magnitude and timing of the digitized values of the calorimeter signal.

### Acknowledgments

It is a pleasure to acknowledge the many useful and enlightening discussions we have had with Veljko Radeka and Sergio Rescia throughout the course of this work. We have also profited from many useful comments from our colleagues in other endeavors involving liquid argon calorimetry, among whom are C. Fabjan, H. Gordon, D. Lissauer, F. E. Paige, and W. Willis. We are indebted to C. de La Taille for bringing to our attention the important role of quantization errors in this analysis. The work was begun under the SSC Generic Detector R&D Program and continued under the R&D program for the GEM experiment. DOE funding was provided under Contract No.DE-AC02-80ER10667 and Grant No. DE-FG02-90ER40646 at the University of Pittsburgh.

### References

1. W. E. Cleland, E. A. Scholle, and E. G. Stern, "Pileup and thermal noise in a liquid ionization calorimeter" in *Symposium on Detector Research and Development for the Superconducting Supercollider*, Ft. Worth, Texas, October 15-18, 1990, p. 318.
2. W. E. Cleland and E. G. Stern "Signal Processing Considerations for Liquid Ionization Calorimeters in a High Rate Environment", to be submitted to Nucl. Inst. and Methods, 1992.
3. V. Radeka and S. Rescia, Nucl. Inst. and Methods A265, 228 (1988).
4. V. Radeka, Ann. Rev. Nucl. Sci. 38, 217; (1988).
5. J. Freeman and C. Newman-Holmes, "A Fast Calorimeter Simulation for SSC Detector Design," *Proceedings from the Workshop on Detector Simulation for the SSC*, ANL-HEP-CP-88-51, L. Price ed., Argonne National Labs, 1988, p. 285.
6. R. K. Bock et al., Nucl. Inst. and Methods 186, 533 (1981).

7. A. Papoulis, *Signal Analysis*, (McGraw Hill, 1976), p. 324.
8. E. Gatti, P. Rehak, and M. Sampietro, Nucl. Inst. and Methods;A274,469;(1989).

## DISCLAIMER